Visible-light-driven photocatalytic degradation of sulfamethazine by surface engineering of carbon nitride：Properties, degradation pathway and mechanisms

Chengyun Zhou[a,1], Zhuotong Zeng[b,1], Guangming Zeng[a*], Danlian Huang[a*], Rong Xiao[b*], Min Cheng[a], Chen Zhang[a], Weiping Xiong[a], Cui Lai[a], Yang Yang[a], Wenjun Wang[a], Huan Yi[a], Bisheng Li[a]

[a] *College of Environmental Science and Engineering, Hunan University and and Key Laboratory of Environmental Biology and Pollution Control (Hunan University), Ministry of Education, Changsha 410082, P.R. China ;*

[b] *Department of Dermatology, Second Xiangya Hospital, Central South University, Changsha 410011, P R China.*

---

[*] Corresponding author at: College of Environmental Science and Engineering, Hunan University, Changsha, Hunan 410082, China.

Tel.: +86–731– 88822754; fax: +86–731–88823701.

E-mail address: zgming@hnu.edu.cn (G.M. Zeng), xiaorong65@csu.edu.cn (R. Xiao).

[1] These authors contribute equally to this article.

Abstract

Polymeric carbon nitride semiconductor has been explored as emerging metal-free photocatalyst for solving the energy shortage and environmental issues. However, the efficiency of carbon nitride is still not satisfying. Herein, a facile copolymerization between L-cysteine and dicyandiamide has been applied to forming the modified carbon nitride photocatalysts. The photocatalytic performance was evaluated through degrading sulfamethazine under visible light illumination. The ameliorative structure and tuned energy band result in visible-light adsorption enhancement. In addition, nitrogen vacancies offer more sites to adsorbing molecular oxygen, thereby facilitating the transfer of electrons from carbon nitride to the surface adsorbed oxygen. As a result, the degradation rate of optimized modified carbon nitride sample for sulfamethazine was 0.1062 min^{-1}, which was almost 12 times than that of carbon nitride (0.0086 min^{-1}). Superoxide radicals and holes were mainly responsible for the sulfamethazine photodegradation by modified carbon nitride. Two reaction intermediates/products were observed and identified by high performance liquid chromatography-mass spectrometer, and a possible reaction pathway was proposed. This study provides new insights into the design of highly efficient photocatalyst for other organic pollutants degradation.

Key words: Carbon nitride; L-cysteine; Photocatalysis; Sulfamethazine degradation; Nitrogen vacancy.

1. Introduction

Nowadays, environmental pollution caused by various pharmaceuticals has become worldwide issues of increasing concern [1-6]. Pharmaceuticals comprise of a series of different compounds and are constantly released into the environment at low concentration, which present potential adverse effects to wildlife and human health [7-9]. Sulfonamides are a class of typical drugs (antibiotics), which have antibacterial activity and are widely used in human and veterinary medicine [10-14]. They were detected in waste water, surface water, ground water, and the concentration was ranged from 20-1000 ng L^{-1} [15]. It is urgent to develop a simple and efficient method for wastewater purification. The solar photocatalysis could be a promising route to solve the current energy crisis and environmental issues [16-20].

Recent years, organic semiconductors have become the most promising materials for photocatalytic hydrogen generation and degradation of pollutants, such as conjugated microporous polymers, covalent triazine-based frameworks (CTFs) [21-25], and polymeric carbon nitrides (CN) [26-28]. Among these organic semiconductors, CN has attracted significant attention due to its remarkable electronic properties, chemical stability, and cost-effective characters [29]. CN also has potential for large-scale production since it can be produced from commonly available reagents (melamine, dicyandiamide, urea or thiourea) [30-32]. The CN was mainly applied in environmental and energy area, such as water splitting, CO_2 reduction or pollutant degradation [33-37]. CN based catalysts also can produce H_2O_2 under visible light since the 1,4-endoperoxide species on the CN surface converted as H_2O_2 molecule [38, 39]. However, the photocatalytic activity of bulk CN was restricted by insufficient light absorption, small surface area, and short lifetime of photo-exciton.

In this regard, significant advances in CN synthesis and activity as a photocatalyst have been achieved by numerous efforts like copolymerization, doping with different heteroatoms, and heterostructure construction [40-43]. Previous studies indicated that copolymerization carbon nitride precursors with conjugated monomers could enhance the visible light absorption via n-π* electronic transition [44-46]. Traditional graphitic carbon nitride has perfectly symmetric and planar heptazine units, resulting in a π-π* electronic transition [47]. The n-π* electronic transition at the nitrogen atoms with lone pairs was found in some self-assemble disordered copolymers of carbon nitride, which would lead to enlarge the visible light absorption [48, 49]. In addition, nitrogen vacancy defects were also found in modified carbon nitride, which could trap photogenerated electrons, and then depressing the recombination of photogenerated carriers [50]. Considering the advantages of n-π* electronic transition and nitrogen vacancy defects, it can be inferred that the coexistence of nitrogen vacancy defects and n-π* electronic transition may enhance the photocatalytic activity of CN for pollutants degradation [51, 52]. However, there are few studies on the design of a modified carbon nitride with both these two advantages. Furthermore, the application of modified carbon nitride on the SMZ degradation is less studied.

In this work, a naturally occurring amino acid (i.e. L-cysteine) was first selected as a suitable monomer to incorporate with dicyandiamide to obtain the modified carbon nitride (LCN) via facile thermal copolymerization. Further thermal condensation was conducted to exfoliate LCN photocatalyst. For comparison, dicyandiamide-based carbon nitride (DCN) was obtained by only dicyandiamide condensation under identical condition. The incorporated of L-cysteine will affect the intrinsic structure and charge carrier behavior of carbon nitride by creating nitrogen vacancies and disordered structural, and induce the n-π* electronic transition. The L-cysteine modified carbon nitride exhibits superior photocatalytic activity due to the n-π* electronic transition and nitrogen vacancies of modified carbon nitride. Influential factors properties of modified carbon nitride for SMZ degradation have been evaluated. This work provides a facile route for rational design of modified carbon nitride via organic precursor copolymerization. Also, it can be seen that the modified carbon nitride can applied as a potential low-cost, high efficient photocatalyst on water treatment.

2. Experimental section

2.1 Synthesis of LCN and DCN

Dicyandiamide and L-cysteine (Lcy) were obtained from Sinopharm Chemical Reagent Co., Ltd (Shanghai, China). All reagents were analytical grade and used as received without additional purification or treatment. MilliQ ultra-pure water with a resistivity higher than 18.2 MΩ·cm was used in whole experiments.

The modified LCN composites were synthesized from dicyandiamide and L-cysteine with different mass ratios [36]. In a typical preparation process, 3 g of dicyandiamide and a varied amount (i.e. 0.005，0.015, or 0.03 g) of Lcy were first mixed by ball milling. The mixture was then placed in a covered crucible and heated at 550 ℃ for 4 h with a ramp rate of 2.3 ℃ min^{-1}. The as-prepared intermediate stage product was then grinded and placed in an open crucible, followed by heating at 550 ℃ for 2 h with a ramp rate of 10 ℃/min to obtain the final product in a muffle furnace. The yields of the final product were about 0.8 g. The final products were labeled as LCN-x, and x (g) was represented the amount of Lcy. For comparison, DCN was synthesized by repeating the above procedures without adding Lcy [34].

2.2 Characterizations

Powder X-ray diffraction (XRD) patterns of samples was obtained by a Rigaku D/max-2500 instrument with Cu $K\alpha$ radiation (λ = 0.15406 nm). Fourier transform infrared (FT-IR) spectra were recorded in BioRad FTS-600 spectrometer. The morphology of samples was obtained by a FEI Helios NanoLab 600i scanning electron microscopy (SEM) and FEI Tecnai G2F20 transmission electron microscopy (TEM). Brunauer-Emmett-Teller (BET, Micromeritics Instrument Corporation, TRI-STAR3020, USA) was used to evaluate the pore structure of samples. The X-ray photoelectron spectra (XPS) of samples were obtained using an ESCALAB 250Xi spectrometer.

The UV-vis diffuse reflectance spectra (DRS) of samples were measured on a Cary 300UV-vis spectrophotometer. Room temperature Photoluminescence (PL) spectra were obtained at a Perkin Elmer luminescence spectrometer (LS 50 B, E_x=365 nm). The electron spin resonance (ESR) signals of radicals by spin-trapping reagent 5, 5-dimethyl-l-pyrroline N-oxide (DMPO) were analyzed by a Bruker ER200-SRC spectrometer under visible light irradiation (λ> 420 nm).

2.3 Photocatalytic activity tests

Sulfamethazine (SMZ) was used as a probe contaminant in photocatalytic activity studies [46, 47]. Batch pollutants degradation was performed in a 100 mL beaker under magnetic stirring at 450 rpm. Typically, 0.025 g of catalyst sample was dispersed into 50 mL of SMZ stock solution (100 μM) [16]. Before irradiation, dark reaction was conducted to achieve the absorption-desorption equilibrium. The degradation reaction was tested by a xenon lamp (PLS-SXE300, PerfectLight, Beijing) equipped with a 420 nm cut filter at a distance of 0.1 m from the top. The output energy was 300 W and the irradiation intensity was 415 mW cm^{-2}. Control experiments with the absence of catalyst under visible light were also performed under the same condition. Degradation samples were taken out and filtered at an interval time. The concentration of SMZ was determined by an HPLC series 1100 (Agilent, Germany) equipped with a UV-vis detector. C18 column (4.6 × 250 mm) was adopted with the temperature of 30 ℃. The HPLC analysis method for SMZ was based on the previous study and had a mobile phase of 80:20 0.02M acetic acid: methanol, a flow rate of 1 mL min^{-1}, an injection volume of 20 μL, and a 270 nm detection wavelength [36].

2.4 Photoelectrochemical measurements

The photoelectrochemical measurements were performed on a CHI 760E workstation in a three-electrode system, where the catalysts were deposited on a fluorine doped tin oxide (FTO) glass as the working electrode, a Pt plate was used as the counter electrode and an Ag/AgCl (saturated

KCl) was as reference electrode. 0.2 M Na_2SO_4 solution was used as electrolyte [42, 49]. The working electrode was fabricated as follows: 3 mg of sample was dispersed in 1 mL of 0.5 % Nafion water-ethanol solution and sonication for 1 h. Then 50 μL of mixture was dropped on the cleaned FTO glass electrode and further dried at 120 ℃ for 2 h. The photocurrent response and EIS were measured in standard three-electrode system with the 300 W Xe arc lamp with a cut-off filter ($\lambda >$ 420 nm) as the visible light source. Mott-Schottky plots were obtained by three sweeps in a voltage range of −1 - 1 V with amplitude of 10 mV at the selected frequencies of 1.0 kHz.

3. Results and discussion

Typically, carbon nitride synthesized from dicyandiamide is named as DCN and L-cysteine modified CN polymers are named as LCN-x, where x represents the weight of L-cysteine (x=0.005, 0.015, and 0.03).

3.1 Structure, morphology and band structure

In Fig.1a, the typical XRD patterns of LCN-x samples are very similar to DCN, which given two representative peaks at 12.7 ° and 27.4 °. The peak at 12.7 ° corresponds to the in-plane periodic repeat structural, while the peak at 27.4 ° corresponds to the conjugated aromatic systems in (002) graphitic planes of carbon nitride [37, 53, 54]. The (002) peak shows a slight shift from 27.4 °(DCN) to 27.6 °(LCN-0.015) (Fig. 1b), suggesting denser packing sheets in the framework during thermal reaction were obtained. FT-IR results indicated that the chemical structure of LCN-x was almost identical to that of DCN (Fig. 1c). The peak at 809 cm^{-1} on the FT-IR spectrum attributes to the s-triazine units of carbon nitride. The strong peak at 1200 to 1650 cm^{-1} mainly corresponds to the stretching mode of the DCN heptazine cycle [55]. LCN-x samples have similar but broader and less sharp peaks due to the incorporation of oxygen species into the framework. The peak located at 3000 to 3500 cm^{-1} is the stretching vibration of N-H and O-H surface group, which corresponds to the surface residual N–H group and absorbed H_2O molecules, respectively.

The morphology of DCN and LCN-0.015 was studied by TEM and SEM. Since L-cysteine has a linear molecular structure and oxygen-rich functional group, then it could react with dicyanamide by hydrogen bond to form a linear polymer after calcination. When heated in muffle furnace, L-cysteine would be decomposed to SO_2, CO_2 and NH_3. The evolution of gas may greatly accelerate the sluggish deamination process and change the morphology of carbon nitride. These morphology changes were evidenced by TEM images in Fig. 2a and b. It could be found that DCN presents a planar sheet-like structure and LCN-0.015 maintained sheet morphology. Differently, the LCN-0.015 displays curl-like nanostructures with some irregular pores. The SEM image of DCN sample showed dense and stacked morphology (Fig. 2c). After the addition of Lcy and thermal exfoliation process, the image of LCN-0.015 displayed coral-like and hierarchical network structural (Fig. 2d). The distortion in LCN samples allow more n–π* transitions from the edge N atoms to the CB, which might also benefit for the visible photon absorption [48]. The element mapping results confirmed that DCN (Fig. S1) and LCN-0.015 (Fig. S2) were composed of C, N, and O. It can be seen that the atomic ratio of C/N was 0.74 for DCN and 0.81 for LCN-0.015 in EDS, respectively. N_2 adsorption-desorption measurement further supported the structural change. In Fig. S3, it can be found that all samples contained mesoporous due to the typical IV behavior with an H1 type hysteresis loop. Compared to packing-like DCN, the hierarchical structure of LCN-0.015 possesses a higher surface area (from 11 m^2 g^{-1} for DCN to 28 m^2 g^{-1} for LCN-0.015). However, further increasing amount of Lcy, the specific surface area of LCN-0.03 decreased. This is mainly due to the fact that excess Lcy may destroy the intrinsic structure units and cause pore collapse, which could be confirmed by reducing the pore volume from 0.28 to 0.18 cm^3 g^{-1} (Table 1).

With the addition of Lcy, the color of LCN gradually darken and finally turns dark brown (Fig. S4), which reflected to the absorption property by DRS. In Fig. 3a, the optical absorption of DCN was around 460 nm. In comparison, the absorption of LCN-x shifted to longer wavelength (460-700 nm), indicating that the LCN could harvest wide range of visible light. The intrinsic absorption bands below 460 nm may attributed to π-π^* electron transitions in the conjugated aromatic system [35]. However, the absorption bands at about 460-700 nm may be assigned to an n-π^* electron transitions involving single pairs of the edge nitrogen atoms (NH_x) on the heptazine units [48]. Specifically, n-π^* transitions are spatially prohibited for perfectly symmetric carbon nitride, indicating that nitrogen vacancies were formed in dissymmetric planar LCN. The nitrogen vacancies increase in the order of DCN<LCN-0.005<LCN-0.015<LCN-0.03, which can be validated by room-temperature electron paramagnetic resonance (EPR) spectra. In Fig. 3b, all samples showed a central symmetry adsorption peak centered at g=2.003, which are ascribed to the unpaired electrons in the framework of carbon nitride. The EPR intensity was increase in the order of DCN<LCN-0.005<LCN-0.015<LCN-0.03, which was in good agreement with the DRS results.

The band gap of DCN and LCN-0.015 are calculated from Tauc plots (Fig. S5). The band gap of DCN is 2.64 eV, which is larger than LCN-0.015 (2.55 eV). It can be seen that the band gap of LCN was influenced by the additive amount of Lcy. In addition, the LCN has defect sites due to the addition of Lcy. The light absorption increase or band gap decrease leading to the higher photocatalytic activity of LCN samples than DCN.

The XPS survey spectrum indicates the chemical state and surface elements of DCN and LCN-0.015, respectively (Fig. 4a). All samples showed the similar characteristic binding energies of carbon nitride. As shown in Fig. 4b, C1s spectra shows two evident peaks at 284.7 eV and 288.2 eV, which are corresponding to adventitious C-C/C=C bond and sp^2-hybridized carbon N=C-N bonds, respectively . N1s spectra displays four binding species (Fig. 4c) corresponding to sp^2-hybridized nitrogen (C−N=C, 398.7 eV), tertiary nitrogen atoms ($N-(C)_3$, 399.8 eV), terminal amino groups ($-NH_2$, 401.2 eV), and π-excitation (404.2 eV) [56]. It is noteworthy to observe that the area ratio between C−N=C and N−(C)$_3$ reduce from 3.8 to 3.2. The part of C−N=C transform to N−(C)$_3$ may due to the structural distortion. This low value of C−N=C/N−(C)$_3$ indicates that nitrogen vacancies are formed by the adding of Lcy in the carbon nitride framework [57]. The O 1 s spectrum of DCN was fitted into two peaks at 531.7 and 532.9 eV, which are corresponded to the CO$_2$ and adsorbed water, respectively. A new peak at 531.9 eV appeared in LCN-0.015, which is ascribed to C=O-C species (Fig. 4d) [58]. Organic elemental analysis (OEA) was further conducted to confirm the nitrogen vacancies in LCN-x samples. The C/N atomic ratio is 0.65 for DCN and increases to 0.67 and 0.68 for LCN-0.015 and LCN-0.03, respectively (Table S1), which is in good accordance with the EDS analysis and previous surface XPS analysis. This result indicated that the number of nitrogen vacancies was increasing with the increasing amount of Lcy.

3.2 *Photocatalytic activities and degradation products analysis*

The photocatalytic degradation activities of DCN and LCN-x samples were further evaluated by SMZ antibiotics removal under visible light. Dark adsorption/desorption equilibrium test has been taken (Table S2). In Fig. 5a, Blank tests have shown that almost negligible SMZ was degraded in the absence of catalyst. All the as-prepared photocatalysts are active for SMZ degradation under visible light irradiation. Only 39% of SMZ was degraded by DCN after 60 min. All the modified LCN-x samples show improved degradation activities in comparison with the pure DCN, where LCN-0.015 exhibits the highest degradation efficiency (99.7% for 1 h). However, excess amount of Lcy would bring negative effect in photocatalytic activity. This finding demonstrates that excess dopant may damage the conjugated structural of carbon nitride. All the SMZ removal curves fitting the pseudo-first order kinetic equation (Fig. 5b). The apparent SMZ removal rate constant for blank, DCN, LCN-0.005, LCN-0.015 and LCN-0.03 was 0.0003 min^{-1}, 0.0086 min^{-1}, 0.0762 min^{-1}, 0.1062 min^{-1} and 0.0453 min^{-1}, respectively. The photodegradation activity of LCN-0.015 for SMZ removal was about 12 times than that of DCN. Therefore, the modification of Lcy in the carbon nitride was beneficial for enhanced SMZ degradation. After photocatalysis, desorption experiments indicated the SMZ was degraded rather than adsorption. The TOC removal efficiency of SMZ for DCN and LCN-0.015 after 1 h visible light illumination was presented in Fig. S6. In addition, the initial rate of SMZ was found to be equal to 0.59 μmol L^{-1} min^{-1} (λ=420 nm) in Fig. S7 [59-61]. The apparent quantum efficiency of the LCN-0.015 was determined to be 0.2% (λ=420 nm). The adsorption and degradation of SMZ by LCN-0.015 in different pH (i.e. pH=3.0, 6.0, 8.0, 10.0) was shown in Fig. 5c and 5d. The results indicated that the adsorption of SMZ by catalyst was negligible. It can be seen that with the increase of initial pH, the degradation efficiency was enhanced due to the less consumption of $\bullet O_2^-$.

To further explore the photocatalytic removal mechanism of SMZ, the degradation products in the photodegradation process were identified by high performance liquid chromatography-mass spectrometer (HPLC-MS). Possible intermediate products at different reaction time have been added in Fig. S8. The concentration of SMZ (m/z 279.1) decreased with the time prolonging, indicating SMZ was degraded. The intermediate of P1 (m/z 215.1) was increased from 0 min to 30 min and then decreased after 30 min. P1 may formed by the product of SO_2 extrusion of SMZ, a phenomenon frequently presented by sulfonamides [62]. The other intermediate P2 (m/z 124) was appeared in 30 min, but they existed in a low level after 60 min. It can be seen that P2 was produced by the holes attack on the SMZ which resulted in the cleavage of S-N bond on SMZ. Proposed degradation products were listed in Table S3.

In addition, photocatalyst reusability is a key factor for potential practical application. The reusability of LCN-0.015 was tested by four cycles of SMZ degradation tests. From Fig.6a, it can be observed that the kinetic constant of catalyst was decreased from 0.1042 min^{-1} to 0.0921 min^{-1} after four run cycles. This decrease was due to the degradation products cover the surface of catalyst and occupy the reactive sites of catalyst. Furthermore, the used LCN-0.015 sample was further characterized by XRD, FT-IR and SEM analysis. Based on XRD spectra (Fig. 6b) and FT-IR spectra (Fig. 6c) results, the phase and chemical structure of LCN-0.015 was keep after cycle tests. Compared to fresh catalyst, the SEM morphology of used LCN-0.015 exhibits no remarkable difference (Fig. 6d). In addition, this photocatalyst exhibited higher photocatalytic activity when compared with other catalysts (Table S4). These results demonstrate that the high stability of the LCN-0.015 photocatalyst has been designed successfully for its potential practical applications.

3.3 Visible light catalytic activity enhancement mechanism

To evaluate the degree of improvement in separation and transfer of charge carriers, photoluminescence spectroscopy measurements have been conducted. The mechanism of enhanced photocatalytic activity of LCN-x was further studied by photoelectrochemical measurements. In Fig. 7a，it presents the transient photocurrent response of DCN and LCN-x samples under visible light irradiation. All samples were stable during the cycle of light on and light off. In the tested samples, the LCN-0.015 showed the highest photocurrent. The photocurrent density of LCN-0.015 (1.90 μA cm^{-2}) showed a 27-fold higher than that of DCN (0.07 μA cm^{-2}), indicating that better separation and transfer rate of the photogenerated charge carriers were obtained in LCN-0.015. In addition, the EIS analysis was further preceded in the dark condition (Fig. 7b). The arc radius of LCN-0.015 sample is smaller than that of DCN, indicating that the resistance of LCN-0.015 is less than that of DCN. The results also indicate that the photoelectrochemical properties of LCN-0.015 were enhanced, which is consistent with the photocurrent test. The above electronic properties indicate that the modification of Lcy can enhance the separation and transfer of charge, which is advantageous for promoting photocatalytic activity.

As shown in Fig. 7c，DCN showed a strong PL peak located at around 460 nm, which was derived from the inter-band recombination of charge carriers [63]. Compared with DCN, LCN-0.015 showed a weaker PL intensity, indicating that the recombination of charge carriers in the carbon nitride framework has been suppressed. This result indicated the separation efficiency of charge carries in the LCN-x was improved, which may favor to the potential photocatalytic reaction. Furthermore, the LCN-x showed a red-shift of the PL maximum peaks from 460 to 471 nm, which is consistent with the band gap reduction of these samples. Time resolved fluorescence spectra were also collected to explain the charge separation of the samples in Fig. 7d. Fitting results were given in Table 2. The lifetime (t) of DCN was 6.88 ns, while it is 5.19 ns for LCN-0.015. This reduced singlet lifetime indicates enhanced exciton dissociation, which facilitated the hot charge carrier transfer and yield.

To detect the active species of LCN-0.015 in the photocatalytic degradation, ESR and radical trapping experiments were carried out. The superoxide radical (•O_2^-) and hydroxyl radical (•OH) can be detected by ESR. As shown in Fig. 8a, DMPO-•O_2^- has a strong signal under visible light irradiation, while no obvious signal was observed in dark. Meanwhile, a weak four-line spectrum with 1:2:2:1 was observed in the DMPO-water solution, which was identified the signal of DMPO-•OH (Fig. 8b). The results can also be confirmed by trapping tests. In Fig. 8c the photodegradation of SMZ with the addition of different kinds of excess scavengers (tertiary butanol (tBuOH) for •OH, 4-hydroxy-2,2,6,6-tetramethylpiperidineN-oxyl (TEMPOL) for •O_2^- and ethylenediaminetetraacetic acid disodium (EDTA-2Na) for holes). The addition of tBuOH has little effect on photocatalytic activity of SMZ. However, when the TEMPOL and EDTA-2Na are added into the reaction, the degradation efficiency of SMZ was reduced from 99% to 22% and 46%, respectively. Trapping experiments indicated that •O_2^- and h^+ active radicals were the main active species, which are in good agreement with the above-mentioned ESR results and previous reports [64-66].

To identify the possible band gap structure of DCN and LCN-0.015, Mott-Schottky plot carried out. The Mott-Schottky plots of DCN and LCN-0.015 present a positive slope, indicating they are n-type semiconductor. The LCN-0.015 has a higher charge carrier density than DCN due to the lower slope of LCN-0.015. From the linear part of Mott-Schottky polts, the flat band potential of LCN-0.015 was -1.04 V *vs.* Ag/AgCl, while the DCN was -1.21 V *vs.* Ag/AgCl (Fig. S9). The results of VB-XPS were consistent with those from Mott–Schottky plots (Fig. S10). For n-type semiconductor, the flat band potential is close to the conduction band (CB) level. Valence band position can be obtained by subtracting the band gap values. Relative band position of DCN and LCN-0.015 are presented in Fig. 9a. The mechanism was investigated from two aspects. One was the photocatalytic generation of H_2O_2 and the other was the photocatalytic degradation of SMZ. Under visible light illumination, band gap excitation generates the electron-hole pairs. The electrons on the surface of LCN-0.015 can reduce the dissolved oxygen to active $•O_2^−$. The holes on the LCN-0.015 cannot oxidize the OH^- to •OH due to the VB potential was lower than the potential of $•OH/OH^−$ (1.99 eV). This photocatalyst also could activate molecular oxygen to generate H_2O_2 and also decompose the in-situ-generated H_2O_2 to produce •OH for SMZ degradation (Fig. 9b). In addition, holes can also directly decompose the pollutants. These results were in good agreement with trapping and ESR results.

4. Conclusions

In summary, this work gives ideas for the designing of high-efficient carbon nitride photocatalyst by using dicyandiamide and L-cysteine and applied it into the water treatment. After Lcy modification, the chemical composition showed minor changes, while the optical absorption, electronic properties and nanostructure were optimized. The photoelectrochemical characterization and PL results also indicated that the disordered LCN was more efficient in separating charge carriers and inducing exciton dissociation. As a result, the optimized LCN-0.015 showed the enhanced activities for the oxidation of SMZ antibiotics when compared with those of DCN. Intermediates of SMZ degradation were identified by HPLC-MS, and the degradation pathway was also proposed. Based on the radical scavenger test and ESR results, the $\bullet O_2^-$ and holes are the main radical species in the degradation process of SMZ for LCN-0.015 sample. In future work, theoretical calculations should be as a guide to rational design the modified carbon nitride. In addition, more co-monomers should be developed to design high efficient photocatalysts. Before carbon nitride practically application, it is critical to improve the stability of carbon nitride in long-runs reactions. Immobilization of carbon nitride and combination of carbon nitride with other photocatalysts will decrease the photocatalyst leaching, enlarge the light absorption, and enhance the charge carriers' separation for reactions.

Acknowledgements

This study was financially supported by the Program for the National Natural Science Foundation of China (81773333,51879101, 51809090, 51579098, 51779090, 51709101, 51709100, 51278176, 51521006, 51378190), the National Program for Support of Top-Notch Young Professionals of China (2014), the Fundamental Research Funds for the Central Universities, Hunan Provincial Science and Technology Plan Project (No. 2016RS3026, 2017SK2243, 2018SK20410), the Program for New Century Excellent Talents in University (NCET-13-0186), the Fundamental Research Funds for the Central Universities (531109200027, 531107051080, 531107050978, 531107051205), Hunan Provincial Innovation Foundation For Postgraduate (CX2018B195), Shanghai Tongji Gao Tingyao Environmental Science and Technology Development Foundation, and the Program for Changjiang Scholars and Innovative Research Team in University (IRT-13R17).

References

[1] S. Zhong, C. Zhou, X. Zhang, H. Zhou, H. Li, X. Zhu, Y. Wang, A novel molecularly imprinted material based on magnetic halloysite nanotubes for rapid enrichment of 2, 4-dichlorophenoxyacetic acid in water, J. Hazar. Mater. 276 (2014) 58-65.

[2] C. Zhou, H. Li, H. Zhou, H. Wang, P. Yang, S. Zhong, Water﹣compatible halloysite﹣imprinted polymer by Pickering emulsion polymerization for the selective recognition of herbicides, J. Sep. Sci. 38 (2015) 1365-1371.

[3] J.-L. Gong, B. Wang, G.-M. Zeng, C.-P. Yang, C.-G. Niu, Q.-Y. Niu, W.-J. Zhou, Y. Liang, Removal of cationic dyes from aqueous solution using magnetic multi-wall carbon nanotube nanocomposite as adsorbent, J. Hazar. Mater. 164 (2009) 1517-1522.

[4] P. Xu, G.M. Zeng, D.L. Huang, C.L. Feng, S. Hu, M.H. Zhao, C. Lai, Z. Wei, C. Huang, G.X. Xie, Z.F. Liu, Use of iron oxide nanomaterials in wastewater treatment: A review, Sci. Total Environ. 424 (2012) 1-10.

[5] S. Ye, G. Zeng, H. Wu, C. Zhang, J. Dai, J. Liang, J. Yu, X. Ren, H. Yi, M. Cheng, Biological technologies for the remediation of co-contaminated soil, Crit. Rev. Env. Sci. Tec. 37 (2017) 1062-1076.

[6] L. Zhang, J. Zhang, G. Zeng, H. Dong, Y. Chen, C. Huang, Y. Zhu, R. Xu, Y. Cheng, K. Hou, Multivariate relationships between microbial communities and environmental variables during co-composting of sewage sludge and agricultural waste in the presence of PVP-AgNPs, Bioresource Technol 261 (2018) 10-18.

[7] S. Ye, G. Zeng, H. Wu, C. Zhang, J. Liang, J. Dai, Z. Liu, W. Xiong, J. Wan, P. Xu, Co-occurrence and interactions of pollutants, and their impacts on soil remediation—A review, Crit. Rev. Env. Sci. Tec. 47 (2017) 1528-1553.

[8] Y. Song, J. Tian, S. Gao, P. Shao, J. Qi, F. Cui, Photodegradation of sulfonamides by g-C_3N_4 under visible light irradiation: Effectiveness, mechanism and pathways, Appl. Catal. B: Environ.210 (2017) 88-96.

[9] X. Tang, G. Zeng, C. Fan, M. Zhou, L. Tang, J. Zhu, J. Wan, D. Huang, M. Chen, P. Xu, Chromosomal expression of CadR on Pseudomonas aeruginosa for the removal of Cd(II) from

aqueous solutions, Sci. Total Environ. 636 (2018) 1355-1361.

[10] X. Ren, G. Zeng, L. Tang, J. Wang, J. Wan, H. Feng, B. Song, C. Huang, X. Tang, Effect of exogenous carbonaceous materials on the bioavailability of organic pollutants and their ecological risks, Soil Biol. Biochem. 116 (2018) 70-81.

[11] W. Xiong, Z. Zeng, X. Li, G. Zeng, R. Xiao, Z. Yang, Y. Zhou, C. Zhang, M. Cheng, L. Hu, C. Zhou, L. Qin, R. Xu, Y. Zhang, Multi-walled carbon nanotube/amino-functionalized MIL-53(Fe) composites: Remarkable adsorptive removal of antibiotics from aqueous solutions, Chemosphere 210 (2018) 1061-1069.

[12] M. Cheng, G. Zeng, D. Huang, C. Lai, Y. Liu, C. Zhang, R. Wang, L. Qin, W. Xue, B. Song, S. Ye, H. Yi, High adsorption of methylene blue by salicylic acid–methanol modified steel converter slag and evaluation of its mechanism, J. Colloid Interf. Sci. 515 (2018) 232-239.

[13] C. Zhang, C. Lai, G. Zeng, D. Huang, C. Yang, Y. Wang, Y. Zhou, M. Cheng, Efficacy of carbonaceous nanocomposites for sorbing ionizable antibiotic sulfamethazine from aqueous solution, Water Res. 95 (2016) 103-112.

[14] L. Qin, D. Huang, P. Xu, G. Zeng, C. Lai, Y. Fu, H. Yi, B. Li, C. Zhang, M. Cheng, C. Zhou, X. Wen, In-situ deposition of gold nanoparticles onto polydopamine-decorated g-C_3N_4 for highly efficient reduction of nitroaromatics in environmental water purification, J Colloid Interface Sci 534 (2019) 357-369.

[15] W. Xiong, G. Zeng, Z. Yang, Y. Zhou, C. Zhang, M. Cheng, Y. Liu, L. Hu, J. Wan, C. Zhou, R. Xu, X. Li, Adsorption of tetracycline antibiotics from aqueous solutions on nanocomposite multi-walled carbon nanotube functionalized MIL-53 (Fe) as new adsorbent, Sci. Total Environ. 627 (2018) 235-244.

[16] C. Zhou, C. Lai, P. Xu, G. Zeng, D. Huang, C. Zhang, M. Cheng, L. Hu, J. Wan, Y. Liu, W. Xiong, Y. Deng, M. Wen, In Situ Grown AgI/$Bi_{12}O_{17}Cl_2$ Heterojunction Photocatalysts for Visible

Light Degradation of Sulfamethazine: Efficiency, Pathway, and Mechanism, ACS Sus. Chem. Eng. 6 (2018) 4174-4184.

[17] Y. Yang, Z. Zeng, C. Zhang, D. Huang, G. Zeng, R. Xiao, C. Lai, C. Zhou, H. Guo, W. Xue, M. Cheng, W. Wang, J. Wang, Construction of iodine vacancy-rich BiOI/Ag@AgI Z-scheme heterojunction photocatalysts for visible-light-driven tetracycline degradation: Transformation pathways and mechanism insight, Chem. Eng. J. 349 (2018) 808-821.

[18] Y. Yang, C. Zhang, C. Lai, G. Zeng, D. Huang, M. Cheng, J. Wang, F. Chen, C. Zhou, W. Xiong, BiOX (X = Cl, Br, I) photocatalytic nanomaterials: Applications for fuels and environmental management, Advances in Colloid and Interface Science 254 (2018) 76-93.

[19] D. Huang, C. Hu, G. Zeng, M. Cheng, P. Xu, X. Gong, R. Wang, W. Xue, Combination of Fenton processes and biotreatment for wastewater treatment and soil remediation, Sci. Total Environ. 574 (2017) 1599-1610.

[20] B. Shao, X. Liu, Z. Liu, G. Zeng, Q. Liang, C. Liang, Y. Cheng, W. Zhang, Y. Liu, S. Gong, A novel double Z-scheme photocatalyst $Ag_3PO_4/Bi_2S_3/Bi_2O_3$ with enhanced visible-light photocatalytic performance for antibiotic degradation, Chem. Eng. J. 368 (2019) 730-745.

[21] H. Wang, Z. Zeng, P. Xu, L. Li, G. Zeng, R. Xiao, Z. Tang, D. Huang, L. Tang, C. Lai, D. Jiang, Y. Liu, H. Yi, L. Qin, S. Ye, X. Ren, W. Tang, Recent progress in covalent organic framework thin films: fabrications, applications and perspectives, Chem Soc Rev 48 (2019) 488-516.

[22] C. Zhou, C. Lai, C. Zhang, G. Zeng, D. Huang, M. Cheng, L. Hu, W. Xiong, M. Chen, J. Wang, Y. Yang, L. Jiang, Semiconductor/boron nitride composites: Synthesis, properties, and photocatalysis applications, Appl. Catal. B: Environ.238 (2018) 6-18.

[23] K. He, G. Chen, G. Zeng, A. Chen, Z. Huang, J. Shi, T. Huang, M. Peng, L. Hu, Three-dimensional graphene supported catalysts for organic dyes degradation, Appl. Catal. B: Environ. 228 (2018) 19-28.

[24] L. Qin, G. Zeng, C. Lai, D. Huang, P. Xu, C. Zhang, M. Cheng, X. Liu, S. Liu, B. Li, “Gold rush” in modern science: Fabrication strategies and typical advanced applications of gold nanoparticles in sensing, Coordin. Chem. Rev. 359 (2018) 1-31.

[25] H. Yi, D. Huang, L. Qin, G. Zeng, C. Lai, M. Cheng, S. Ye, B. Song, X. Ren, X. Guo, Selective prepared carbon nanomaterials for advanced photocatalytic application in environmental pollutant treatment and hydrogen production, Appl. Catal. B: Environ.239 (2018) 408-424.

[26] J. Barrio, A. Grafmüller, J. Tzadikov, M. Shalom, Halogen-hydrogen bonds: A general synthetic approach for highly photoactive carbon nitride with tunable properties, Appl. Catal. B: Environ.237 (2018) 681-688.

[27] D.K.L. Chan, J.C. Yu, Facile synthesis of carbon- and oxygen-rich graphitic carbon nitride with enhanced visible-light photocatalytic activity, Catal. Today 310 (2018) 26-31.

[28] G. Li, J. Shi, G. Zhang, Y. Fang, M. Anpo, X. Wang, The facile synthesis of graphitic carbon nitride from amino acid and urea for photocatalytic H_2 production, Res. Chem. Intermediat. 43 (2017) 5137-5152.

[29] W.J. Ong, L.L. Tan, Y.H. Ng, S.T. Yong, S.P. Chai, Graphitic Carbon Nitride (g-C3N4)-Based Photocatalysts for Artificial Photosynthesis and Environmental Remediation: Are We a Step Closer To Achieving Sustainability?, Chem Rev 116 (2016) 7159-7329.

[30] M. Zhang, X. Wang, Two dimensional conjugated polymers with enhanced optical absorption and charge separation for photocatalytic hydrogen evolution, Energ. Environ. Sci. 7 (2014) 1902.

[31] D. Huang, X. Yan, M. Yan, G. Zeng, C. Zhou, J. Wan, M. Cheng, W. Xue, Graphitic Carbon Nitride-Based Heterojunction Photoactive Nanocomposites: Applications and Mechanism Insight, ACS Appl Mater Interfaces 10 (2018) 21035-21055.

[32] D. Huang, Z. Li, G. Zeng, C. Zhou, W. Xue, X. Gong, X. Yan, S. Chen, W. Wang, M. Cheng, Megamerger in photocatalytic field: 2D g-C_3N_4 nanosheets serve as support of 0D nanomaterials

for improving photocatalytic performance, Appl. Catal. B: Environ. 240 (2019) 153-173.

[33] J. Qin, S. Wang, H. Ren, Y. Hou, X. Wang, Photocatalytic reduction of CO_2 by graphitic carbon nitride polymers derived from urea and barbituric acid, Appl. Catal. B: Environ.179 (2015) 1-8.

[34] L. Jiang, X. Yuan, G. Zeng, Z. Wu, J. Liang, X. Chen, L. Leng, H. Wang, H. Wang, Metal-free efficient photocatalyst for stable visible-light photocatalytic degradation of refractory pollutant, Appl. Catal. B: Environ. 221 (2018) 715-725.

[35] G. Zhang, G. Li, Z.A. Lan, L. Lin, A. Savateev, T. Heil, S. Zafeiratos, X. Wang, M. Antonietti, Optimizing Optical Absorption, Exciton Dissociation, and Charge Transfer of a Polymeric Carbon Nitride with Ultrahigh Solar Hydrogen Production Activity, Angewandte Chemie 129 (2017).

[36] C. Zhou, C. Lai, D. Huang, G. Zeng, C. Zhang, M. Cheng, L. Hu, J. Wan, W. Xiong, M. Wen, X. Wen, L. Qin, Highly porous carbon nitride by supramolecular preassembly of monomers for photocatalytic removal of sulfamethazine under visible light driven, Appl. Catal. B: Environ. 220 (2018) 202-210.

[37] W. Wang, P. Xu, M. Chen, G. Zeng, C. Zhang, C. Zhou, Y. Yang, D. Huang, C. Lai, M. Cheng, L. Hu, W. Xiong, H. Guo, M. Zhou, Alkali Metal-Assisted Synthesis of Graphite Carbon Nitride with Tunable Band-Gap for Enhanced Visible-Light-Driven Photocatalytic Performance, ACS Sus. Chem. Eng. 6 (2018) 15503-15516.

[38] S. Zhao, X. Zhao, Polyoxometalates-derived metal oxides incorporated into graphitic carbon nitride framework for photocatalytic hydrogen peroxide production under visible light, J. Catal. 366 (2018) 98-106.

[39] Y. Shiraishi, S. Kanazawa, Y. Kofuji, H. Sakamoto, S. Ichikawa, S. Tanaka, T. Hirai, Sunlight-Driven Hydrogen Peroxide Production from Water and Molecular Oxygen by Metal-Free Photocatalysts, Angewandte Chemie International Edition 53 (2014) 13454-13459.

[40] C. Zhou, C. Lai, P. Xu, G. Zeng, D. Huang, Z. Li, C. Zhang, M. Cheng, L. Hu, J. Wan, F. Chen,

W. Xiong, R. Deng, Rational Design of Carbon-Doped Carbon Nitride/Bi$_{12}$O17Cl2 Composites: A Promising Candidate Photocatalyst for Boosting Visible-Light-Driven Photocatalytic Degradation of Tetracycline, ACS Sus. Chem. Eng. 6 (2018) 6941-6949.

[41] W. Ho, Z. Zhang, W. Lin, S. Huang, X. Zhang, X. Wang, Y. Huang, Copolymerization with 2,4,6-triaminopyrimidine for the rolling-up the layer structure, tunable electronic properties, and photocatalysis of g-C_3N_4, ACS Appl Mater Interfaces 7 (2015) 5497-5505.

[42] X. Fan, L. Zhang, R. Cheng, M. Wang, M. Li, Y. Zhou, J. Shi, Construction of Graphitic C3N4-Based Intramolecular Donor–Acceptor Conjugated Copolymers for Photocatalytic Hydrogen Evolution, ACS Catal. 5 (2015) 5008-5015.

[43] H. Ou, X. Chen, L. Lin, Y. Fang, X. Wang, Biomimetic Donor-Acceptor Motifs in Conjugated Polymers for Promoting Exciton Splitting and Charge Separation, Angew Chem Int Ed Engl 57 (2018) 8729-8733.

[44] Z. Zhou, Y. Zhang, Y. Shen, S. Liu, Y. Zhang, Molecular engineering of polymeric carbon nitride: advancing applications from photocatalysis to biosensing and more, Chem Soc Rev 47 (2018) 2298-2321.

[45] J. Zhang, X. Chen , K. Takanabe, K. Maeda, K. Domen, J.D. Epping, X. Fu, M. Antonietti, X. Wang Synthesis of a Carbon Nitride Structure for Visible-Light Catalysis by Copolymerization, Angew Chem Int Ed 49 (2010) 441-444.

[46] C. Zhou, D. Huang, P. Xu, G. Zeng, J. Huang, T. Shi, C. Lai, C. Zhang, M. Cheng, Y. Lu, A. Duan, W. Xiong, M. Zhou, Efficient visible light driven degradation of sulfamethazine and tetracycline by salicylic acid modified polymeric carbon nitride via charge transfer, Chem. Eng. J. 370 (2019) 1077-1086.

[47] C. Zhou, P. Xu, C. Lai, C. Zhang, G. Zeng, D. Huang, M. Cheng, L. Hu, W. Xiong, X. Wen, L. Qin, J. Yuan, W. Wang, Rational design of graphic carbon nitride copolymers by molecular doping

for visible-light-driven degradation of aqueous sulfamethazine and hydrogen evolution, Chem. Eng. J. 359 (2019) 186-196.

[48] H. Kim, S. Gim, T.H. Jeon, H. Kim, W. Choi, Distorted Carbon Nitride Structure with Substituted Benzene Moieties for Enhanced Visible Light Photocatalytic Activities, ACS Appl Mater Interfaces 9 (2017) 40360-40368.

[49] Y. Yu, W. Yan, W. Gao, P. Li, X. Wang, S. Wu, W. Song, K. Ding, Aromatic ring substituted g-C3N4 for enhanced photocatalytic hydrogen evolution, Journal of Materials Chemistry A 5 (2017) 17199-17203.

[50] G. Zhang, A. Savateev, Y. Zhao, L. Li, M. Antonietti, Advancing the n [rightward arrow] [small pi]* electron transition of carbon nitride nanotubes for H_2 photosynthesis, J. Mater. Chem. A 5 (2017) 12723-12728.

[51] P. Qiu, C. Xu, H. Chen, F. Jiang, X. Wang, R. Lu, X. Zhang, One step synthesis of oxygen doped porous graphitic carbon nitride with remarkable improvement of photo-oxidation activity: Role of oxygen on visible light photocatalytic activity, Appl. Catal. B: Environ.206 (2017) 319-327.

[52] S. Li, G. Dong, R. Hailili, L. Yang, Y. Li, F. Wang, Y. Zeng, C. Wang, Effective photocatalytic H_2O_2 production under visible light irradiation at g-C_3N_4 modulated by carbon vacancies, Appl. Catal. B: Environ. 190 (2016) 26-35.

[53] Y. Yang, C. Zhang, D. Huang, G. Zeng, J. Huang, C. Lai, C. Zhou, W. Wang, H. Guo, W. Xue, R. Deng, M. Cheng, W. Xiong, Boron nitride quantum dots decorated ultrathin porous g-C_3N_4: Intensified exciton dissociation and charge transfer for promoting visible-light-driven molecular oxygen activation, Appl. Catal. B: Environ. 245 (2019) 87-99.

[54] M. Zhang, W. Jiang, D. Liu, J. Wang, Y. Liu, Y. Zhu, Y. Zhu, Photodegradation of phenol via C_3N_4 -agar hybrid hydrogel 3D photocatalysts with free separation, Appl. Catal. B: Environ. 183 (2016) 263-268.

[55] W. Che, W. Cheng, T. Yao, F. Tang, W. Liu, H. Su, Y. Huang, Q. Liu, J. Liu, F. Hu, Z. Pan, Z. Sun, S. Wei, Fast Photoelectron Transfer in (Cring)–C_3N_4 Plane Heterostructural Nanosheets for Overall Water Splitting, J. Am. Chem. Soc. 139 (2017) 3021-3026.

[56] J. Ding, W. Xu, H. Wan, D. Yuan, C. Chen, L. Wang, G. Guan, W.-L. Dai, Nitrogen vacancy engineered graphitic C_3N_4-based polymers for photocatalytic oxidation of aromatic alcohols to aldehydes, Appl. Catal. B: Environ. 221 (2018) 626-634.

[57] J. Cao, W. Nie, L. Huang, Y. Ding, K. Lv, H. Tang, Photocatalytic activation of sulfite by nitrogen vacancy modified graphitic carbon nitride for efficient degradation of carbamazepine, Appl. Catal. B: Environ. 241 (2019) 18-27.

[58] Y. Wu, H. Wang, Y. Sun, T. Xiao, W. Tu, X. Yuan, G. Zeng, S. Li, J.W. Chew, Photogenerated charge transfer via interfacial internal electric field for significantly improved photocatalysis in direct Z-scheme oxygen-doped carbon nitrogen/CoAl-layered double hydroxide heterojunction, Appl. Catal. B: Environ. 227 (2018) 530-540.

[59] Y. Hong, Y. Jiang, C. Li, W. Fan, X. Yan, M. Yan, W. Shi, In-situ synthesis of direct solid-state Z-scheme V_2O_5/g-C_3N_4 heterojunctions with enhanced visible light efficiency in photocatalytic degradation of pollutants, Appl. Catal. B: Environ. 180 (2016) 663-673.

[60] C. Zhang, W. Wang, A. Duan, G. Zeng, D. Huang, C. Lai, X. Tan, M. Cheng, R. Wang, C. Zhou, W. Xiong, Y. Yang, Adsorption behavior of engineered carbons and carbon nanomaterials for metal endocrine disruptors: Experiments and theoretical calculation, Chemosphere 222 (2019) 184-194.

[61] S. Zhang, L. Wang, C. Liu, J. Luo, J. Crittenden, X. Liu, T. Cai, J. Yuan, Y. Pei, Y. Liu, Photocatalytic wastewater purification with simultaneous hydrogen production using MoS_2 QD-decorated hierarchical assembly of ZnIn2S4 on reduced graphene oxide photocatalyst, Water Res 121 (2017) 11-19.

[62] M. Cheng, G. Zeng, D. Huang, C. Lai, Y. Liu, C. Zhang, J. Wan, L. Hu, C. Zhou, W. Xiong, Efficient degradation of sulfamethazine in simulated and real wastewater at slightly basic pH values using Co-SAM-SCS /H_2O_2 Fenton-like system, Water Res 138 (2018) 7-18.

[63] Z. Wei, F. Liang, Y. Liu, W. Luo, J. Wang, W. Yao, Y. Zhu, Photoelectrocatalytic degradation of phenol-containing wastewater by TiO_2/g-C_3N_4 hybrid heterostructure thin film, Appl. Catal. B: Environ. 201 (2017) 600-606.

[64] Z. Wan, G. Zhang, X. Wu, S. Yin, Novel visible-light-driven Z-scheme $Bi_{12}GeO_{20}$ /g-C_3N_4 photocatalyst: Oxygen-induced pathway of organic pollutants degradation and proton assisted electron transfer mechanism of Cr(VI) reduction, Appl. Catal. B: Environ. 207 (2017) 17-26.

[65] L. Tang, J. Wang, G. Zeng, Y. Liu, Y. Deng, Y. Zhou, J. Tang, J. Wang, Z. Guo, Enhanced photocatalytic degradation of norfloxacin in aqueous Bi_2WO_6 dispersions containing nonionic surfactant under visible light irradiation, J. Hazar. Mater. 306 (2016) 295-304.

[66] H. Wang, X. Yuan, Y. Wu, G. Zeng, X. Chen, L. Leng, Z. Wu, L. Jiang, H. Li, Facile synthesis of amino-functionalized titanium metal-organic frameworks and their superior visible-light photocatalytic activity for Cr(VI) reduction, J. Hazar. Mater. 286 (2015) 187-194.

Figure captions:

Fig. 1 (a) Powder XRD patterns, (b) magnification of the corresponding (002) peak, (c) FT-IR spectra of DCN and LCN-x samples

Fig. 2 TEM images of (a) DCN and (b) LCN-0.015, SEM images of (c) DCN and (d) LCN-0.015.

Fig. 3 (a) UV−visible light absorption spectra, (b) EPR spectra of DCN and LCN-x samples

Fig. 4 High-resolution XPS spectra of (a) survey, (b) C 1s, (c) N 1s and (d) O 1s for DCN and LCN-0.015.

Fig. 5 (a) Photocatalytic degradation of SMZ, (b) degradation rate of SMZ on DCN and LCN-x samples, (c) Effect of initial solution pH for SMZ adsorption by LCN-0.015, and (d) Effect of initial solution pH for SMZ photodegradation by LCN-0.015.

Fig. 6 (a) Kinetic rates of the LCN-0.015 toward the degradation of SMZ under visible light irradiation over four cycles, (b) XRD spectra, (c) FT-IR spectra of fresh and used LCN-0.015, and (d) SEM image of used LCN-0.015.

Fig. 7 (a) Transient photocurrent, (b) electrochemical impedance spectroscopy (EIS) Nyquist plots of DCN and LCN-x samples, (c) Room temperature steady state photoluminescence (PL) emission spectra and (d) time-resolved fluorescence decay spectra of DCN and LCN-x sample with an excitation wavelength of 365 nm.

Fig. 8 ESR spectra of LCN-0.015 dispersion under both the dark and visible light irradiation (> 420 nm) condition: (a) in methanol dispersion for DMPO-$\bullet O_2^-$, (b) in aqueous dispersion for DMPO-$\bullet$OH, (c) reactive species trapping experiments of LCN-0.015 under visible light irradiation.

Fig. 9 Schematic illustrations of electronic band structure for DCN and LCN-0.015 (a), possible mechanism for photocatalytic degradation of SMZ over LCN-0.015 (b).

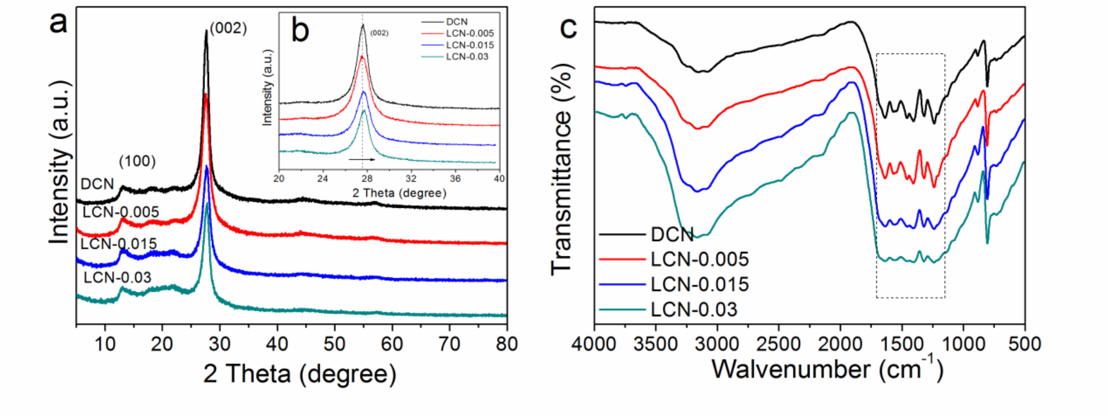

Fig. 1 (a) Powder XRD patterns, (b) magnification of the corresponding (002) peak, (c) FT-IR spectra of DCN and LCN-x samples

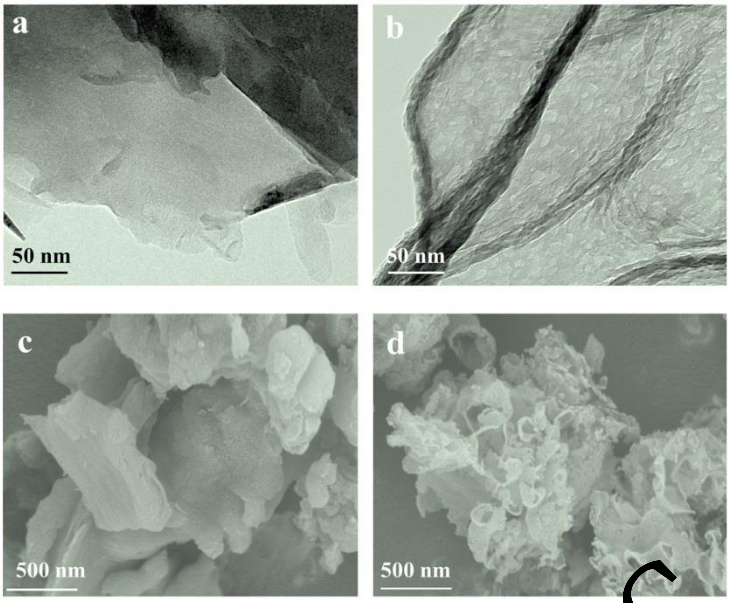

Fig. 2 TEM images of (a) DCN and (b) LCN-0.015, SEM images of (c) DCN and (d) LCN-0.015.

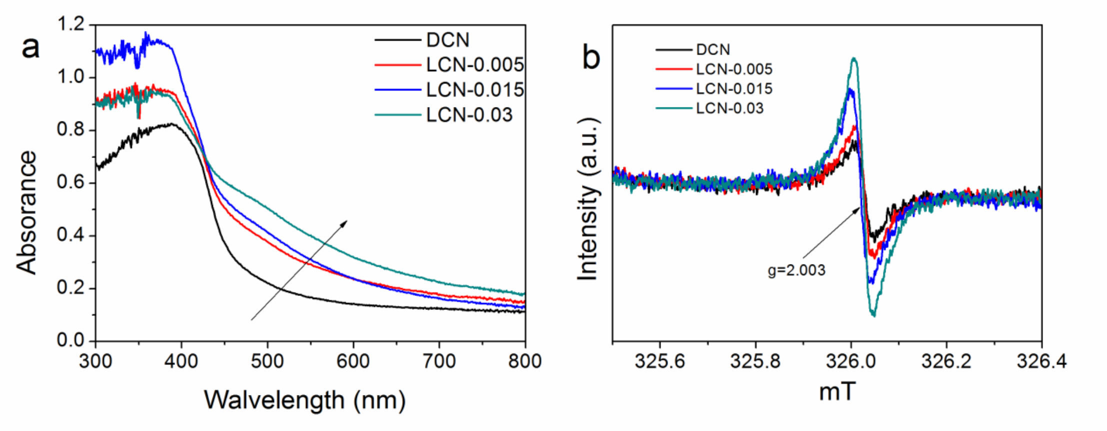

Fig. 3 (a) UV−visible light absorption spectra, (b) EPR spectra of DCN and LCN-x samples

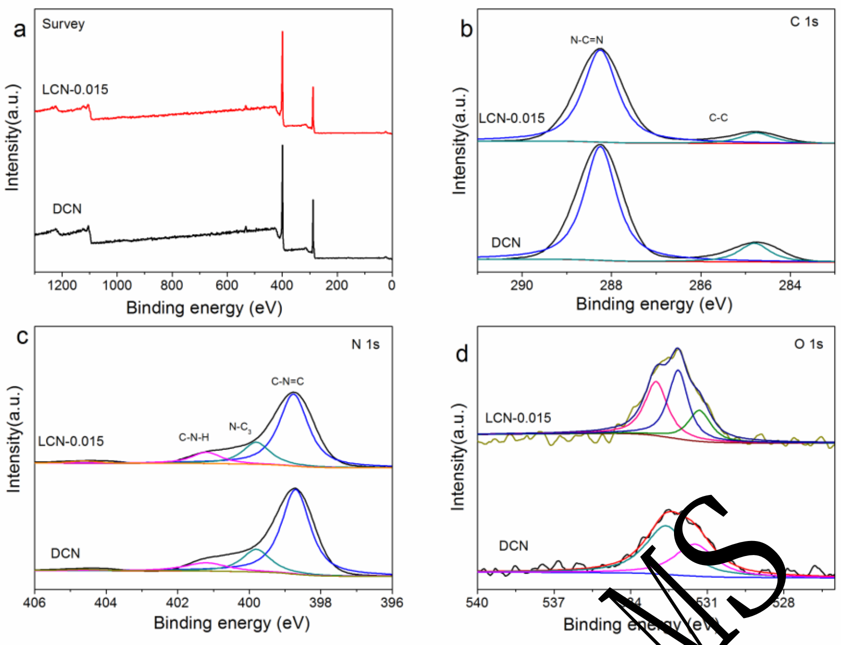

Fig. 4 High-resolution XPS spectra of (a) survey, (b) C 1s, (c) N 1s and (d) O 1s for DCN and LCN-0.015.

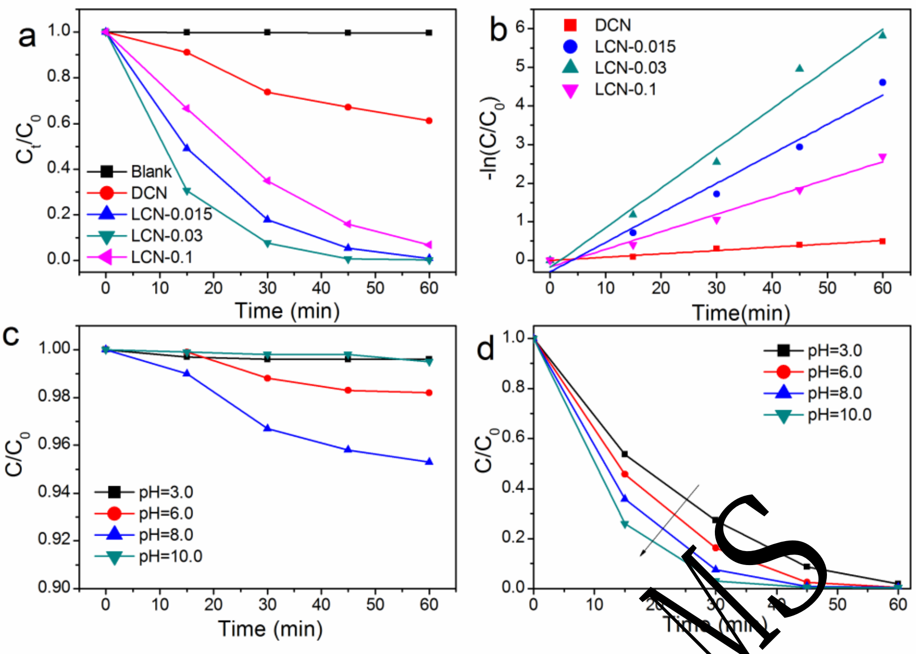

Fig. 5 (a) Photocatalytic degradation of SMZ, (b) degradation rate of SMZ on DCN and LCN-x samples, (c) Effect of initial solution pH for SMZ adsorption by LCN-0.015, and (d) Effect of initial solution pH for SMZ photodegradation by LCN-0.015.

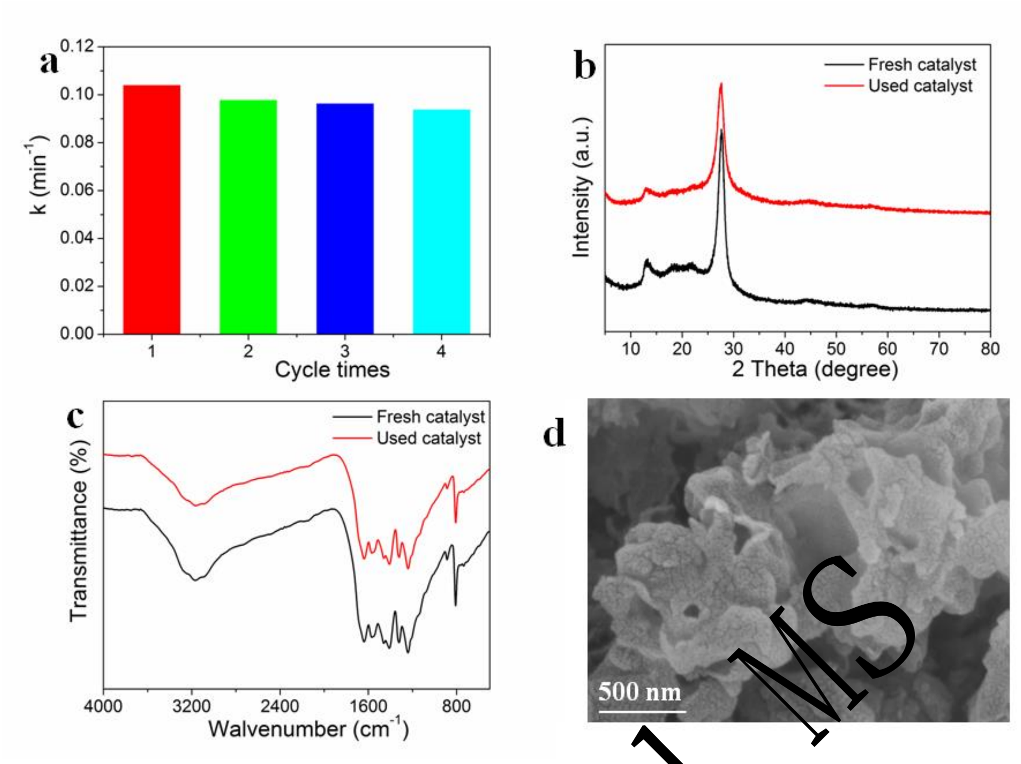

Fig. 6 (a) Kinetic rates of the LCN-0.015 toward the degradation of SMZ under visible light irradiation over four cycles, (b) XRD spectra, (c) FT-IR spectra of fresh and used LCN-0.015, and (d) SEM image of used LCN-0.015.

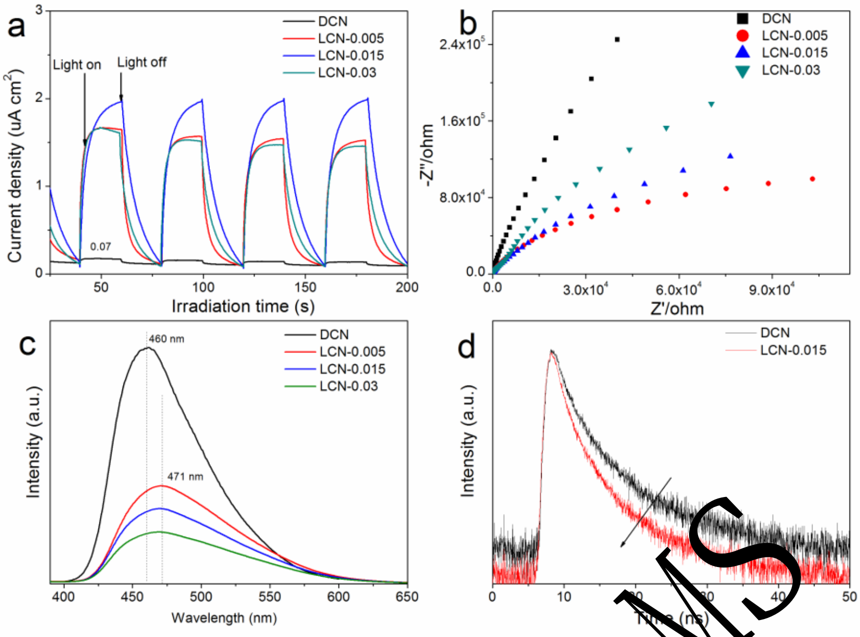

Fig. 7 (a) Transient photocurrent, (b) electrochemical impedance spectroscopy (EIS) Nyquist plots of DCN and LCN-x samples, (c) Room temperature steady-state photoluminescence (PL) emission spectra and (d) time-resolved fluorescence decay spectra of DCN and LCN-x sample with an excitation wavelength of 365 nm.

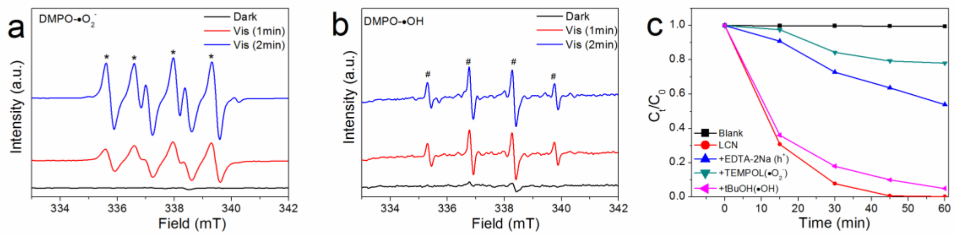

Fig. 8 ESR spectra of LCN-0.015 dispersion under both the dark and visible light irradiation (> 420 nm) condition: (a) in methanol dispersion for DMPO-•O_2^-, (b) in aqueous dispersion for DMPO-•OH, (c) reactive species trapping experiments of LCN-0.015 under visible light irradiation.

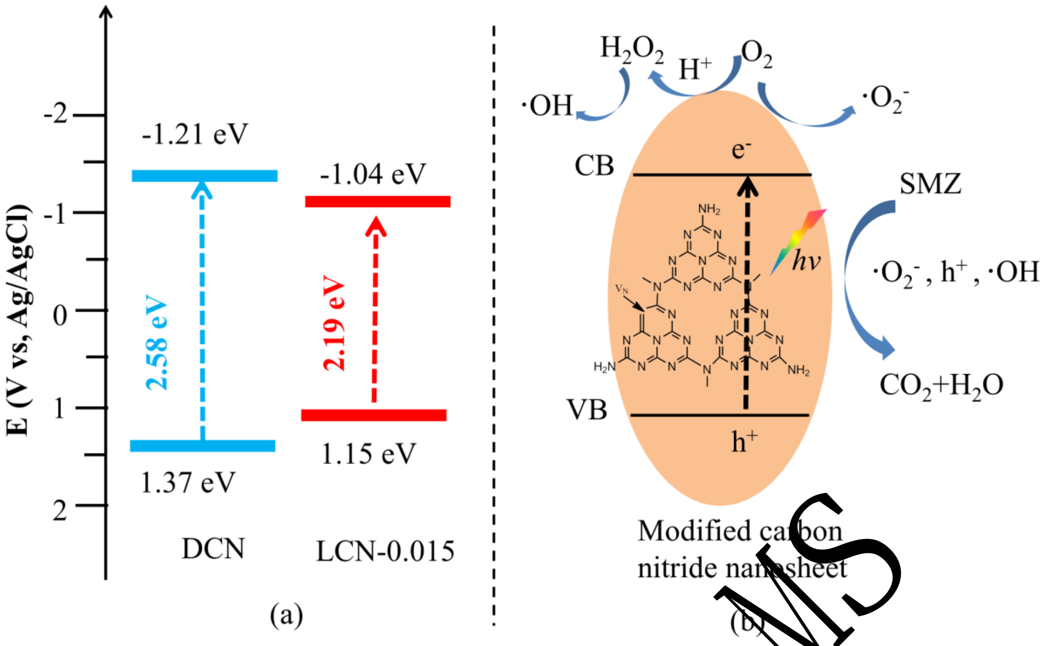

Fig. 9 Schematic illustrations of electronic band structures for DCN and LCN-0.015 (a); possible mechanism for photocatalytic degradation of SMZ over LCN-0.015 (b).

Table 1 surface area and pore volume for PCN and LCN-x samples.

Samples	Surface area (m^2 g^{-1})	Pore volume (cm^3 g^{-1})
DCN	11.53	0.08
LCN-0.005	41.02	0.28
LCN-0.015	28.84	0.18
LCN-0.03	24.93	0.18

Table 2 Dynamics analysis of emission decay for different samples. (τ represents lifetime and A represents relative amplitude)

Sample	τ_1 (ns)	A_1 (%)	τ_2 (ns)	A_2 (%)	$\tau_{average}$(ns)
DCN	2.06	54.4	8.31	45.6	6.88
LCN-0.015	1.56	56.96	6.37	43.04	5.19

The average lifetime was calculated using equation. $\tau_{average}=(A_1\tau_1^2 + A_2\tau_2^2)/ (A_1\tau_1 + A_2\tau_2)$.